



This is a repository copy of *Magnet Eddy Current Loss Reduction in Permanent Magnet Machines*.

White Rose Research Online URL for this paper:
<http://eprints.whiterose.ac.uk/146190/>

Version: Accepted Version

Article:

Ma, J. and Zhu, Z.Q. orcid.org/0000-0001-7175-3307 (2019) Magnet Eddy Current Loss Reduction in Permanent Magnet Machines. *IEEE Transactions on Industry Applications*, 55 (2). pp. 1309-1320. ISSN 0093-9994

<https://doi.org/10.1109/TIA.2018.2874350>

© 2018 IEEE. Personal use of this material is permitted. Permission from IEEE must be obtained for all other users, including reprinting/ republishing this material for advertising or promotional purposes, creating new collective works for resale or redistribution to servers or lists, or reuse of any copyrighted components of this work in other works. Reproduced in accordance with the publisher's self-archiving policy.

Reuse

Items deposited in White Rose Research Online are protected by copyright, with all rights reserved unless indicated otherwise. They may be downloaded and/or printed for private study, or other acts as permitted by national copyright laws. The publisher or other rights holders may allow further reproduction and re-use of the full text version. This is indicated by the licence information on the White Rose Research Online record for the item.

Takedown

If you consider content in White Rose Research Online to be in breach of UK law, please notify us by emailing eprints@whiterose.ac.uk including the URL of the record and the reason for the withdrawal request.



eprints@whiterose.ac.uk
<https://eprints.whiterose.ac.uk/>

Magnet Eddy Current Loss Reduction in Permanent Magnet Machines

Jie Ma and Z. Q. Zhu, Fellow, IEEE

Abstract— Magnet eddy current loss is very important for any types of permanent magnet machines, especially for high-speed permanent magnet machine since it increases significantly with rotating speed and has a great effect on the temperature of magnet, and hence, the electromagnetic performance, as well as irreversible demagnetization of the magnet. In this paper, a new method is proposed to reduce the rotor permanent magnet eddy current loss. The auxiliary slots with optimized size and position are proposed. By this mean, the asynchronous spatial harmonics caused by the armature reaction and the conventional slots can be partially decreased by the harmonics produced by the introduced auxiliary slots. It is proved that the rated on-load magnet eddy current loss can be reduced as much as 81.5% by this method while the rated on-load torque is only decreased by 4.8% in the 3-slot/2-pole machine. In addition, it also shows that the proposed method could offer better performance in a machine with relative larger airgap length and it is also effective for other slot/pole combinations.

Index Terms—Auxiliary slots, high speed PM machine, magnet eddy current loss.

I. INTRODUCTION

THE interest of high speed permanent magnet (HSPM) machine has grown significantly recently due to its high efficiency, high power density, as well as small size [1]-[8]. However, as a consequence of asynchronously rotating harmonics, the magnet eddy current loss is caused by the spatial harmonics as well as the time harmonics, which have significant influence on the machine performance [9]. This part of loss is much more important for high speed machines since it increases with rotating speed significantly, and affects the temperature of magnet, and hence the output torque and efficiency, as well as the potentially irreversible demagnetization of permanent magnets.

In terms of spatial harmonics reduction, many different methods are proposed in the last decades. Winding optimization is one of the most effective ways since a proper winding design can reduce the MMF harmonics of armature field effectively [10]-[13]. However, this method might lead to low winding factor so that the copper loss will be increased to obtain the same output torque. Moreover, the length of end winding is also increased when the winding is overlapped. As a result, the nature frequency of shaft could be decreased, which

may cause mechanical problem when machine operates under high speed condition [14].

Another method is using a relatively large air-gap, which is also desirable for high speed machine in terms of mechanical and aerodynamic considerations [15]. Since the high order spatial harmonics decay very quickly with the airgap, the large air-gap can filter most of them. However, the output torque is also reduced significantly by this method. Skewing and segmentation are the other two common choices [16]-[21]. Nevertheless, both these two methods are characterized as complicated manufacturing process as well as high cost [22].

In addition, optimization of rotor shape can also offer good performance. [23], [24] present two different rotor shapes for magnet eddy current loss reduction. However, both of them are designed for an interior permanent magnet (IPM) machine, and there might be a mechanical problem if they are employed for a surface mounted permanent magnet (SMPM) machine due to the bending effect and edge effect appearing on the edge of magnets [25]. In contrast, stator structure optimization is more suitable for high speed SMPM machines since the geometry of rotor will not be modified. [22] shows that slot opening with optimized size and position can reduce eddy current loss. However, the reduction is only as much as 15%. In addition, inserting auxiliary slots in the middle of stator teeth can reduce the no-load magnet eddy current loss dramatically [26]. Nevertheless, the influence of armature field is not considered in this method. Consequently, it has very limited influence under rated on-load condition. The adoption of auxiliary slots with optimized size and position are proposed in [27], which could significantly decrease the magnet eddy current loss. Nevertheless, it only focuses on the specific machine topologies, i.e. 3-slot/2-pole machines.

This paper proposes a new method to reduce the magnet eddy current loss by using auxiliary slots. Both size and position of auxiliary slots are optimized under rated working condition. By this method, the asynchronous harmonics produced by armature field and conventional slots can be partially compensated by the harmonics produced by auxiliary slots. The 3-slot/2-pole machine with concentrated windings is chosen as the prototype machine and investigated at first due to its simple structure. Then the influences of airgap length and slot/pole combinations are studied as well.

This paper is organized as follows. In Section II, the air-gap flux density in a conventional 3-slot/2-pole permanent magnet machine is analyzed, both PM and armature fields are considered. In Section III, the effect of auxiliary slots on

magnet eddy current loss is investigated and validated by the finite element (FE) method. Then, in Section IV, the electromagnetic performance of machine with auxiliary slots is evaluated and compared with the conventional machine. The influence of different working conditions is investigated in Section V. In addition, the effects of airgap length and slot/pole combinations are investigated in Section VI and Section VII, respectively. Finally, in Section VIII, the experiments are carried out for verifying part of numerically predictions, e.g. the back EMF as well as the static torque.

II. FIELD ANALYSIS IN 3-SLOT 2-POLE PERMANENT MAGNET MACHINES

In order to understand the source of asynchronous spatial harmonics in 3-slot/2-pole machine, the air-gap magnetic field analysis is very necessary. In this section, the air-gap flux density is calculated by a simple magnetomotive force (MMF)-permeance model which has several assumptions.

1) The saturation of stator lamination is not considered. In addition, since this model is only for explaining the working mechanism of the proposed method instead of giving the accurate solution, the tangential flux component is neglected as well.

- 2) The relative recoil permeability of PM is the same as air.
- 3) Negligible eddy current reaction.
- 4) The flux leakage and end effect are neglected.

A 3-slot/2-pole conventional PM machine with concentrated winding is selected as the prototype machine shown in Fig.1, and its detailed parameters are listed in Table I. It should be noticed that in order to ease the investigation, the thickness of sleeve is also included in the airgap length which will not be calculated and presented separately.

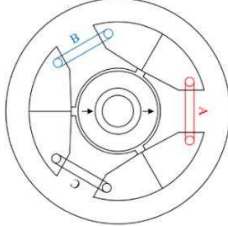


Fig. 1. Cross section of 3-slot/2-pole surface mounted permanent magnet machine.

TABLE I
BASIC PARAMETERS OF MACHINE

| | | | |
|----------------------------|-----|----------------------------|----------|
| Slot number | 3 | Shaft diameter (mm) | 7 |
| Pole number | 2 | Magnet thickness (mm) | 3.8 |
| Stator outer diameter (mm) | 50 | Magnet material | Nd-Fe-B |
| Stator inner diameter (mm) | 19 | Magnetization | Parallel |
| Stator yoke height (mm) | 5.2 | Remanence (T) | 1.2 |
| Slot opening (mm) | 2 | Rated current (A) | 10 |
| Air-gap length (mm) | 1 | Current angle (Elec. Deg.) | 0 |
| Rotor outer diameter (mm) | 17 | Rated speed (rpm) | 60000 |
| Axial length (mm) | 30 | Number of turns per phase | 32 |

A. Open-Circuit Air-Gap Flux Density

The MMF generated by rotor PM material can be treated as a sinusoidal wave since parallel magnetization is employed in this 2-pole machine. Hence, the MMF can be expressed as a cosine function of air-gap circumferential position θ as well as rotating speed ω .

$$F_{PM}(\theta, t) = F_{PM} \cdot \cos(\theta - \omega t) \quad (1)$$

The air-gap permeance model accounting for stator slots is shown in Fig. 2, and its Fourier series is expressed as

$$P(\theta) = P_0 + P_{kn_r} \sum_{k=1}^{\infty} \cos(kn_r(\theta - \theta_0)) \quad (2)$$

where P_0 is the DC component of permeance, k is the harmonics index, P_{kn_r} is the amplitude of Fourier coefficient for the kn_r th harmonic, n_r is the stator tooth number and θ_0 indicates the phase difference between the initial rotor-pole position and the horizon line.

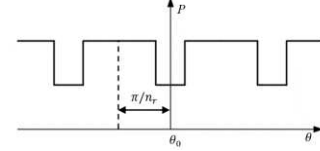


Fig. 2. Air-gap permeance distribution accounting for stator slots.

Therefore, the open-circuit air-gap flux density can be obtained by multiplying the PM MMF and the air-gap permeance distribution

$$\begin{cases} B_{PM}(\theta, t) = F_{PM}(\theta, t) \cdot P(\theta) \\ = P_0 F_{PM} \cdot \cos(\theta - \omega t) + \frac{1}{2} F_{PM} P_{kn_r} \sum_{k=1}^{\infty} (\cos A + \cos B) \\ A = (kn_r + 1)\theta - kn_r\theta_0 - \omega t \\ B = (kn_r - 1)\theta - kn_r\theta_0 + \omega t \end{cases} \quad (3)$$

B. Armature Reaction Air-Gap Flux Density

Fig. 3 shows the MMF distribution when $I_{\text{phaseA}} = 0$ A, where I_{phaseA} indicates the current for phase A, where F indicates the amplitude of MMF and θ indicates the rotor position in mechanical degree. It should be noticed that measurable even order armature MMF harmonics exist in a 3-slot/2-pole machine, which is mainly due to the diametrically asymmetric disposition of the stator slots and coils [28].

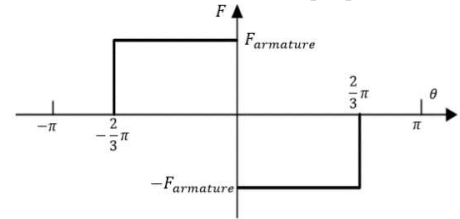


Fig. 3. Air-gap MMF generated by armature field in 3-slot/2-pole SMPM machine ($I_{\text{phaseA}} = 0$ A).

The MMF of 3 phases can be expressed as:

$$\begin{cases} F_a = \sum_{q=1}^{\infty} [F_q \cdot \sin(q\theta)] \cdot \sin(\omega t) \\ F_b = \sum_{q=1}^{\infty} [F_q \cdot \sin(q(\theta - \frac{2\pi}{3}))] \cdot \sin(\omega t - \frac{2\pi}{3}) \\ F_c = \sum_{q=1}^{\infty} [F_q \cdot \sin(q(\theta + \frac{2\pi}{3}))] \cdot \sin(\omega t + \frac{2\pi}{3}) \end{cases} \quad (4)$$

The Fourier series expression of air-gap armature MMF can be calculated as a sum of 3 phases:

$$\left\{ \begin{array}{l} F_{ABC}(\theta, t) = \frac{3}{2} \sum_{q=1}^{\infty} [F_q \cdot \sin(\xi)] \\ \xi = \begin{cases} (n\theta + m\omega t) \cdot -m, n \neq 3r \\ 0, n = 3r \end{cases} \\ m = \begin{cases} -1, n = 3i - 2 \\ 1, n = 3i - 1 \end{cases} \end{array} \right. \quad (5)$$

where ω is the electrical speed, n represents the harmonics order, m indicates that the harmonic has the same rotating direction comparing with fundamental harmonics, and i is any positive integer.

The armature air-gap flux density is the product of armature MMF and air-gap permeance:

$$B_{ABC}(\theta, t) = F_{ABC}(\theta, t) \cdot P(\theta) \\ = \underbrace{\frac{3}{2} P_0 \sum_{q=1}^{\infty} [F_q \cdot \sin(\xi)]}_{\text{MMF harmonics}} + \underbrace{\frac{3}{4} F_q P_{kn} \sum_{q=1}^{\infty} \sum_{k=1}^{\infty} [\sin C + \sin D]}_{\text{MMF-slot harmonics}} \quad (6)$$

$$\left\{ \begin{array}{l} C = \xi + kn_r (\theta - \theta_0) \\ D = \xi - kn_r (\theta - \theta_0) \end{array} \right. \quad (7)$$

$$\left\{ \begin{array}{l} C = (kn_r - pq) \cdot \theta - \omega t - kn_r \theta_0 \\ D = -(kn_r + pq) \cdot \theta - \omega t + kn_r \theta_0 \end{array} \right. \quad (8)$$

where MMF harmonics represent the air-gap flux density harmonics caused by non-sinusoidal armature MMF only, and MMF-slot harmonics indicate the spatial harmonics caused by the interaction of armature MMF harmonics and the permeance variation caused by slots.

C. Resultant Air-Gap Flux Density

It is found that the modified harmonics of B_{ABC} have the same characteristics compared with B_{PM} , which means the same order harmonic in B_{ABC} and B_{PM} have the same frequency as well as rotating direction, and the only difference between them is the amplitude and the phase angle. Hence, the resultant air-gap flux density can be calculated as

$$B_{\text{resultant}} = B_{PM} + B_{ABC} \\ = \sum_{j=1,4,7,\dots} B_j \cdot \sin(j\theta - \omega t + \theta_j) + \sum_{k=2,5,8} B_k \cdot \sin(k\theta + \omega t + \theta_k) \quad (9)$$

where j, k are the harmonic indices; B_j, B_k are the Fourier coefficients of the j th, k th harmonics, while θ_j, θ_k represent the corresponding phases.

III. EFFECT OF AUXILIARY SLOTS ON MAGNET EDDY CURRENT LOSS

The effect of auxiliary slots mainly reflects on the modification of air-gap permeance distribution. Fig. 4 shows the permeance model accounting for both conventional and auxiliary slots.

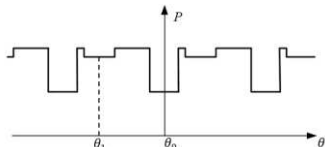


Fig. 4. Air-gap permeance distribution accounting for conventional stator slots and auxiliary slots.

As can be seen, the auxiliary slots have similar effect on permeance modification comparing with the conventional slots. According to (3), (6) and (9), the harmonics produced by auxiliary slots can be also presented in a similar form:

$$B_{\text{har,aux}} = B_{PM,\text{har,aux}} + B_{ABC,\text{har,aux}} \\ = \sum_{j=4,7,11,\dots} B'_j \cdot \sin(j\theta - \omega t + \theta'_j) + \sum_{k=2,5,8} B'_k \cdot \sin(k\theta + \omega t + \theta'_k) \quad (10)$$

where $B_{\text{har,aux}}, B_{PM,\text{har,aux}}$ and $B_{ABC,\text{har,aux}}$ are the total field harmonics, PM field harmonics as well as MMF-slot harmonics caused by auxiliary slots; B'_j, B'_k are the Fourier coefficients of the j th, k th harmonics, while θ'_j, θ'_k represent the corresponding phases.

Since the auxiliary slots affect the air-gap permeance similarly comparing with the conventional slot openings, the harmonics produced by auxiliary slots have the same rotating speed and direction as the harmonics in the conventional machine shown in (3). Meanwhile, with changing the size and position of auxiliary slots, the amplitude and phase of harmonics produced by auxiliary slots can be also modified. Therefore, it is possible to use these harmonics to partially decrease the asynchronous harmonics in the conventional machines so that the magnet eddy current loss can be reduced. Consequently, both optimal size and position of auxiliary slots are required so that the air-gap flux density harmonics produced by them can have the same amplitude but opposite direction comparing with the original asynchronous harmonics.

The finite element (FE) method is employed for global optimization and the magnet eddy current loss calculation. The goal of the optimization is the minimum magnet eddy current loss under rated working condition, and the genetic algorithm is employed in the optimization process. The rated working condition indicates the amplitude of current equals to its rated value, and the current angle is zero, which means the fundamental component of the PM flux linkage is aligned with the d-axis. The optimized parameters are height which may be known as depth, width as well as position of auxiliary slots. The shift angle is defined as the mechanical angle between the middle of the auxiliary slots as well as the middle of corresponding tooth in clockwise direction.

The comparison of topologies of machines with and without auxiliary slots are shown in Fig.5, and the detailed parameters of the optimal auxiliary slots are listed in Table II

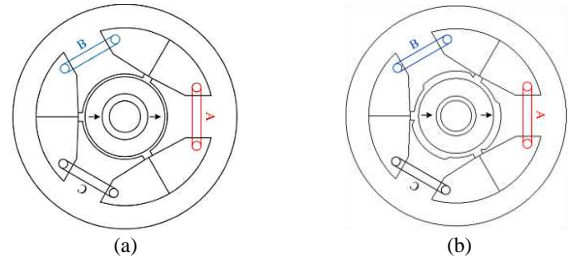


Fig. 5. Cross sections of machine without and with auxiliary slots. (a) Without auxiliary slots. (b) With auxiliary slots.

TABLE II
PARAMETERS OF AUXILIARY SLOT

| | |
|--------------------------|--------|
| Height (mm) | 0.549 |
| Width (mm) | 9.540 |
| Shift angle (Mech. Deg.) | 16.384 |

The magnet eddy current loss is compared in Fig. 6 which can be divided into two different regions. The loss in the region A is lower in the conventional machine, while the opposite trend can be observed in the region B. As can be seen, the magnet eddy current loss under rated working condition, i.e. the current equals to 10A, is reduced by 81.5% in the proposed machine, which shows the great effectiveness of this method.

In order to validate the proposed method further, the 3D FE results are carried out and compared in Fig. 7 and Table III. As shown, the 3D results also confirm the effectiveness of the proposed method. The slight reduction of magnet eddy current loss in 3D FE results is mainly due to the flux leakage in the end part of machine.

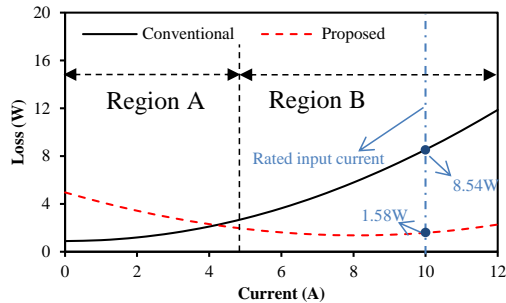


Fig. 6. Average magnet eddy current loss with different currents.

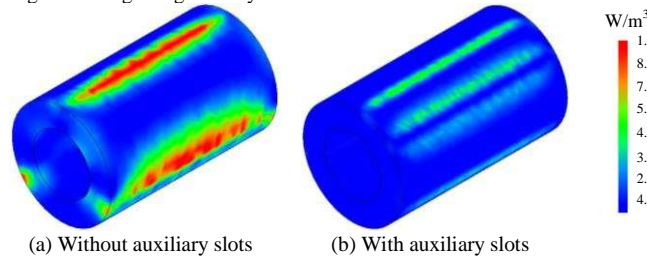


Fig. 7. 3D magnet eddy current loss distribution under rated working condition ($I_{\text{phaseA}}=0$ A).

TABLE III
COMPARISON OF MAGNET EDDY CURRENT LOSS

| | Without auxiliary slots | With auxiliary slots |
|-------------------|-------------------------|----------------------|
| 2D Prediction (W) | 8.54 | 1.58 |
| 3D Prediction (W) | 7.02 | 1.23 |

In order to investigate in details, the spatial harmonics are analyzed and shown in Fig. 8, in which the representative harmonic, i.e. the 2nd spatial harmonic, is selected. In the figure, the first six legends indicate the amplitudes of the 2nd order flux density harmonics from different sources which are corresponded with the left y-axis, and the last two legends indicates the phase difference of the 2nd flux density harmonics between PM and armature fields in conventional and proposed machines which are corresponded with the right y-axis.

As can be seen, the phase differences between the 2nd harmonics in armature and PM fields are about 180 degrees in the proposed machine, which results in a cancelling effect. However, the amplitude of the 2nd harmonic produced by armature reaction is proportional to the input current. Consequently, the cancelling effect is not significant when the input current is low, and the magnet eddy current loss is increased due to the enhanced asynchronous harmonics in PM

field caused by the auxiliary slots. In contrast, the cancelling effect becomes much more significant when the current is higher. Therefore, the magnet eddy current loss is reduced significantly. As for the conventional machine, the phase differences between the 2nd harmonics in PM and armature fields are about 90 degrees. As a result, there is almost no cancelling effect and the harmonics in these two fields nearly add with each other over the whole current interval.

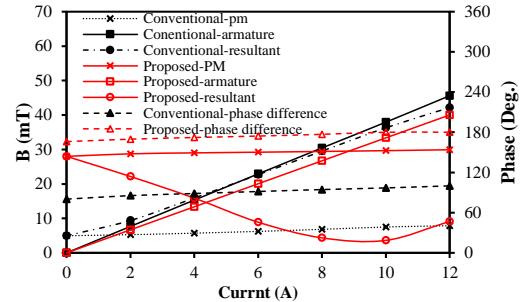


Fig. 8. Variation of the 2nd order flux density harmonic with different current values.

In order to verify that the magnet eddy current loss reduction is due to the spatial harmonics reduction, the comparison of magnet eddy current density distributions is shown in Fig. 9, where α_{rotor} is the rotor circumferential position, H_{PM} is the distance between the radial position of magnet and the central of shaft. The 8.9 mm indicates the outer surface of magnet and 5.1 mm denotes the location of magnet very close to the shaft. It is worth noting that the magnet eddy current density distribution is used instead of flux density distribution. This is due to the fact that the magnet eddy current density distribution considers both amplitude and frequency of spatial harmonics, while the flux density distribution only takes the amplitude of harmonics into account.

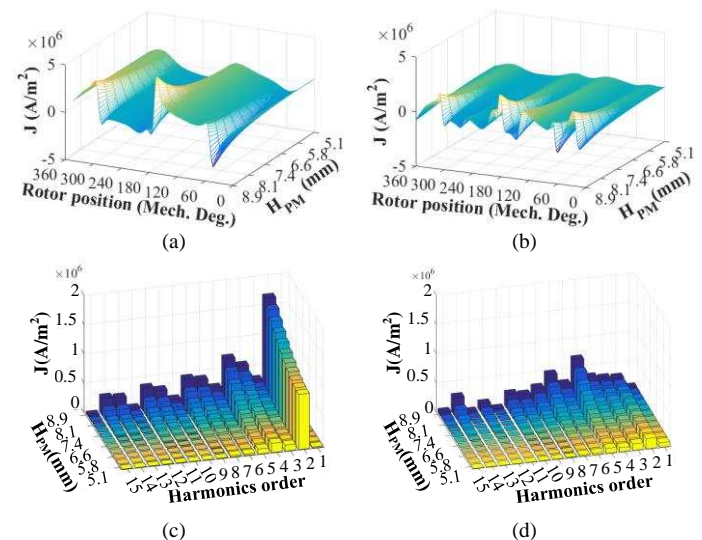


Fig. 9. Eddy current density distribution comparison. (a) and (b) Spatial distributions of machine without and with auxiliary slots. (c) and (d) Spectra of machine without and with auxiliary slots.

As can be seen, the magnet eddy current loss in the conventional machine is mainly caused by low order harmonics, i.e. the 2nd, 4th and 5th harmonics. However, these harmonics are decreased significantly when the auxiliary slots

are added, especially the 2nd harmonic. As a result, the magnet eddy current loss is reduced significantly.

IV. MACHINE PERFORMANCE

In the previous sections, the mechanism and effectiveness of auxiliary slots on the magnet eddy current loss reduction have been explained and investigated. In this section, the electromagnetic performance of the proposed machine is evaluated and compared with the conventional one.

A. Flux Linkage and Back EMF

Fig. 10 compares the open-circuit phase flux linkage. It can be seen that the difference is very small and the slight reduction in the machine with auxiliary slots is mainly due to the increased equivalent air-gap length caused by auxiliary slots.

The phase back EMFs are also compared in Fig. 10. Since the back EMF is proportional to the phase flux linkage.

The impact of auxiliary slots on phase flux linkages is also reflected on the phase back EMFs that the fundamental is reduced slightly. The spectra shows that the harmonic contents in these two machines are very low, which means the auxiliary slots do not introduce extra back EMF harmonics.

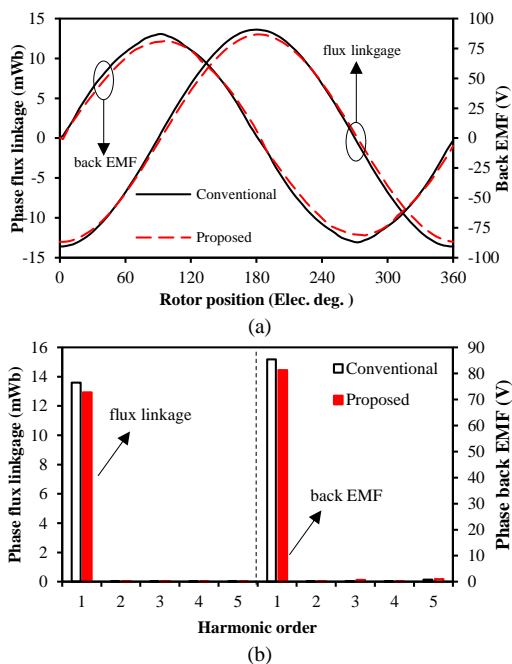


Fig. 10. Phase flux linkage and back EMF comparison. (a) Waveforms. (b) Spectra

B. Torque Characteristics

The cogging torques are compared under no-load condition in Fig. 11. It can be seen that the cogging torques in these two machines have different amplitude as well as phase, which is caused by the shifted auxiliary slots. Moreover, the difference between cogging torques in these two machines is very small, which means the auxiliary slots do not increase the cogging torque significantly.

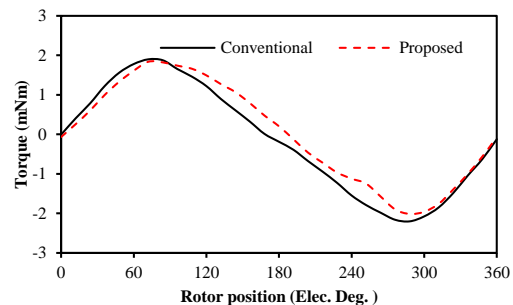


Fig. 11. Cogging torque comparison under no-load condition.

The rated on-load torque of these two machines are shown in Fig. 12. As shown, the output torque of the proposed machine is only reduced slightly, by 4.8%, which is also caused by the increased equivalent air-gap length. In terms of the torque ripple, both these two machines have very low torque ripple since the cogging torque and back EMF harmonics in these two machines with diametric PM magnetization are very low.

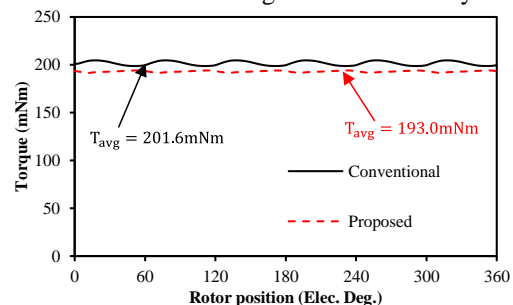


Fig. 12. Rated on-load torque comparison.

C. Unbalanced Magnetic Force

It is well-known that unbalanced magnet force (UMF) occurs in 3-slot/2-pole machine due to the asymmetric stator topology as well as unbalanced winding structure. Fig. 13 shows the UMF comparison, it is found that the UMF is dramatically reduced in the machine with auxiliary slots, and the details will be explained in another paper.

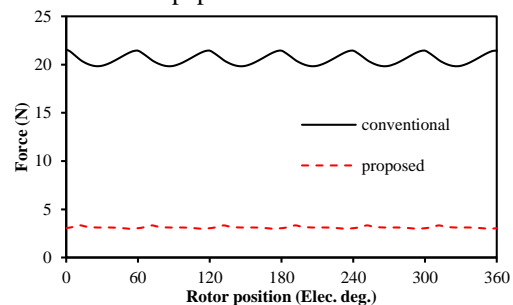


Fig. 13. Unbalanced magnetic force comparison.

V. EFFECT OF WORKING CONDITION

Previous sections focus on the performance evaluation under the rated working condition. However, the working conditions may change in practice. Therefore, the investigation of the effect of working conditions is very necessary.

Fig.14 shows the variations of magnet eddy current loss and on-load average torque with different working conditions. It is found that the loss in the conventional machine increases with current amplitude and the current angle has small influence on its value. In contrast, as for the machine with auxiliary slots, the

minimum magnet eddy current loss occurs around the rated working condition, and the maximum loss occurs when the d-axis current reaches the maximum value. In addition, the machine with auxiliary slots has almost the same output torque comparing with the machine without auxiliary slots under all working conditions, the slight reduction of torque is due to the increased equivalent air-gap caused by auxiliary slots. In contrast, the machine with auxiliary slots has much lower magnet eddy current loss around the rated working condition.

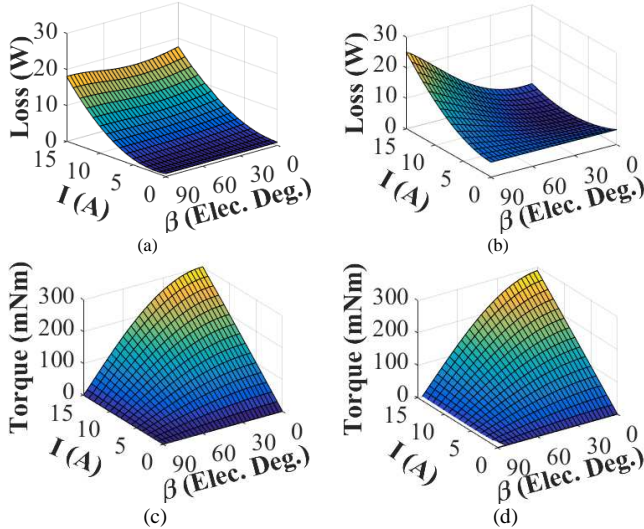


Fig. 14. Performance of machines under different working conditions. (a) and (b) are magnet eddy current loss of machines without and with auxiliary slots. (c) and (d) are torque of machines without and with auxiliary slots.

In order to investigate this phenomenon in more details, the air-gap flux density harmonics with different working conditions are simulated by frozen permeability method [29]. By way of example, the amplitude and phase of the 2nd and 4th harmonics with different input current and current angle are shown in Fig.15 and Fig.16, respectively. It should be noticed that the current angle is fixed as zero in Fig. 15, and the current amplitude is fixed as 10 A in Fig. 16.

It should be mentioned that the other harmonics also have minor effect on the loss. Hence, the amplitudes of 2nd and 4th harmonics of the optimized machine may not be zero under rated working condition. Moreover, although there are only two harmonics analyzed here, but the principle and conclusion can be also applied to any other harmonics.

As can be seen, the effect of current amplitude mainly reflects on the variation of harmonics amplitude caused by armature reaction, while the phase difference between the harmonics produced by PM field and armature field is almost kept as the same. In contrast, when the current angle changes, the phase difference varies dramatically while the amplitude of harmonics are just affected slightly.

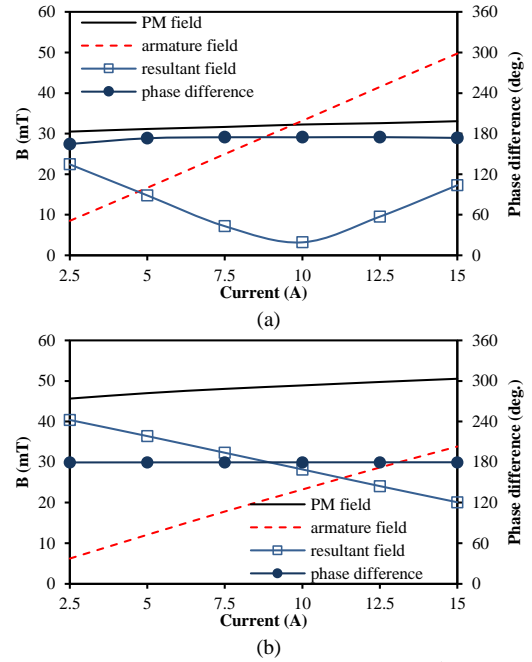


Fig. 15. Harmonics versus different current amplitude. (a) 2nd harmonic. (b) 4th harmonic.

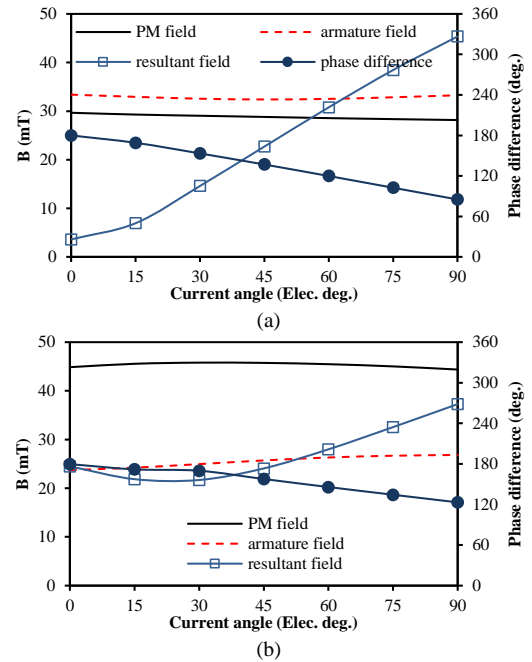


Fig. 16. Harmonics versus different current angle. (a) 2nd harmonic. (b) 4th harmonic.

VI. INFLUENCE OF AIRGAP LENGTH

The previous sections focus on the machines with fixed airgap length. However, the airgap length could be different depending on the rotating speed, materials of sleeve and magnet, etc. Therefore, the influence of airgap length needs to be investigated as well.

Since the main focus for this paper is on the magnet eddy current loss, in order to make fair comparison, the rotor structure and the rotating speed will be kept as the same while the inner diameter of stator will shrink slightly with airgap lengths. The minimum airgap length is chosen as 0.5mm while

the maximum value is 1mm. It is assumed that the mechanical requirement could be met in all situations, since the performance of loss is emphasized.

The auxiliary slots have been optimized with different airgap lengths individually. The rated on-load magnet eddy current loss and torque with different airgap length are shown in Fig.17.

It can be seen that the magnet eddy current loss decreases in both conventional and proposed machines, and it shows that the proposed method could significantly reduce the loss in all different airgap lengths. Moreover, the reduction proportion has also been calculated which is defined as the reduced value over the value in the conventional machine. It can be seen that the reduction proportion of magnet eddy current loss increases with the airgap length from 72.5% to 81.4%, which means the proposed method could offer better performance in terms of the loss reduction in machines having larger airgap length. As for the rated on-load torque, it can be seen that its value decreases with airgap length in both machines, and the difference between the conventional and proposed machines is insensitive to the airgap lengths, of which the variation is smaller than 1%.

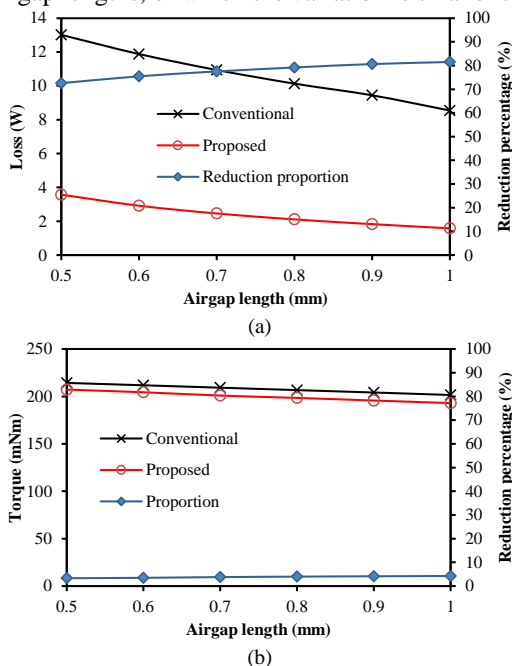


Fig. 17. Machine performances with different airgap lengths. (a) Rated on-load magnet eddy current loss (b) Rated on-load average torque.

The influence of auxiliary slots on the magnet eddy current loss in machines having different airgap lengths mainly depends on the current density harmonic contents on the magnet. The comparison of current densities is shown in Fig.18. The proportion of harmonics of the current density on the PM in conventional and proposed machines with 0.5mm and 1mm airgap lengths are compared, and the reduction due to the auxiliary slots is also shown.

As can be seen, the low order harmonics have larger amplitude, hence more contribution to the loss in machine with 1mm airgap length, especially the 2nd harmonic. This is due to the fact that the high order harmonics have relatively smaller skin depth and the larger airgap length could filter out part of

them. As a result, the higher order harmonics have more influence on the loss in machine with smaller airgap length comparing with the larger one.

However, as shown in Fig. 18 (c), the auxiliary slots mainly reduce the low order harmonics, which means it has very small influence on the high order harmonics. Consequently, the machines with larger airgap length could benefit more in terms of the magnet loss reduction from the proposed method.

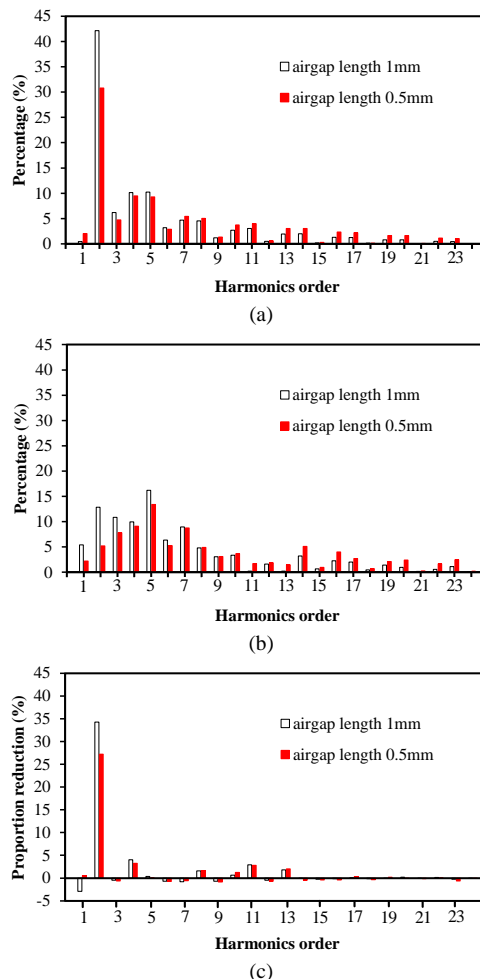


Fig. 18. Harmonic percentage of current density on the PM with different airgap length. (a) Conventional machine (b) Proposed machine. (c) Harmonic reduction by auxiliary slots.

VII. INFLUENCE OF SLOT/POLE COMBINATIONS AND WINDING CONFIGURATIONS

The previous sections investigated the influence of auxiliary slots on the magnet eddy current loss in a 3-slot/2-pole machine. Nevertheless, other slot/pole combinations could be also applied to high speed permanent magnet machines. The feasibility of the proposed method applied to 6-slot/2-pole machines is studied in this section. Both full pitch and tooth-coil windings are taken into account.

The conventional 6-slot/2-pole machines are shown in Fig.19 and the detailed parameters are shown in Table IV. It should be mentioned that these two machines share the same rotor which has the same parameters listed in previous sections, but the stators have been optimized for maximum rated on-load

torque individually due to the different winding configurations. In addition, the input current is fixed as 10A for both machines during the optimization, which means the output torques of machines with different winding structures should be also different.

In terms of auxiliary slots, the sizes and positions are optimized for minimum magnet eddy current loss in both machines separately. The optimized machine topologies are shown in Fig. 20, and the detailed optimal auxiliary slots parameters are listed in Table V.

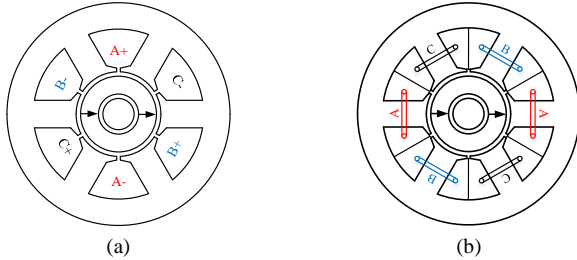


Fig. 19. Cross sections of conventional 6-slot/2-pole machines. (a) With full pitch winding. (b) With tooth-coil winding.

TABLE IV

BASIC PARAMETERS OF 6-SLOT MACHINES

| Parameters | Full pitch winding | tooth-coil winding |
|-------------------------|--------------------|--------------------|
| Stator tooth width (mm) | 5.93 | 5.63 |
| Stator yoke height (mm) | 3.09 | 2.96 |
| Slot opening (mm) | 0.41 | 0.41 |
| Tooth tip height (mm) | 0.82 | 0.55 |

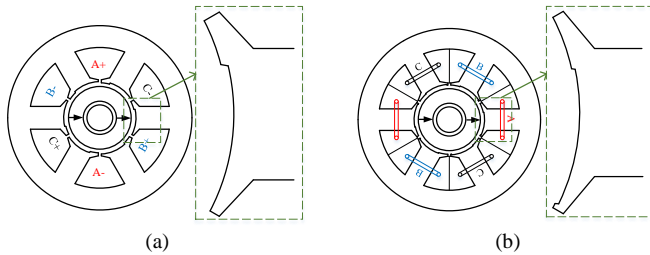


Fig. 20. Cross sections of 6-slot/2-pole machines with optimal auxiliary slots. (a) With full pitch winding. (b) With tooth-coil winding.

TABLE V

BASIC PARAMETERS OF OPTIMAL AUXILIARY SLOTS IN 6-SLOT MACHINE

| Parameters | Full pitch winding | Tooth-coil winding |
|--------------------------|--------------------|--------------------|
| Height (mm) | 0.27 | 0.13 |
| Width (mm) | 6.83 | 5.86 |
| Shift angle (Mech. Deg.) | 6.51 | 7.74 |

The comparison of magnet eddy current losses is shown in Fig. 21. As can be seen, the auxiliary slots can significantly reduce the magnet eddy current loss in both machines. The reductions in machines with full pitch and tooth-coil windings are as much as 82.4% and 78.7% under rated working condition, respectively. Moreover, the machine having tooth-coil winding has lower magnet eddy current comparing with the machine with full pitch winding, which benefits from the lower armature field spatial harmonics caused by the lower winding factor. The total winding factor for the prototype machine with full pitch winding is 1 for all harmonics, while it is 0.5 for all harmonics in the prototype machine with tooth-coil winding.

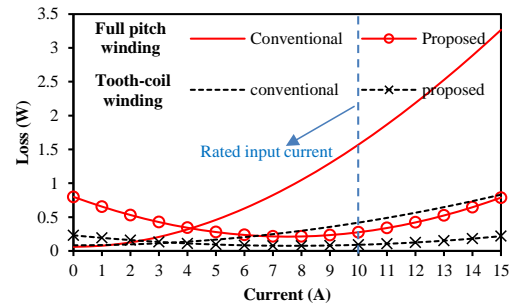


Fig. 21. Magnet eddy current loss of 6-slot/2-pole machines with different currents.

The current density with different magnet thicknesses and rotor positions are shown in Fig. 22 and Fig. 23. As shown, the magnet eddy current loss in 6-slot machines mainly comes from the 5th, 7th, 11th, and 13th spatial harmonics, and the auxiliary slots could reduce these harmonics significantly, and hence much lower magnet eddy current loss.

However, the lower winding factor in machine with tooth-coil winding also results in lower output torque. The comparison of rated on-load torque is shown in Fig. 24. As can be seen, the torque of the machine with full pitch winding is almost twice comparing with the machine having tooth-coil winding.

In terms of the torque reduction due to the auxiliary slots, the torque decreases by 1.2% in the machine with tooth-coil winding but 2.6% in machine with full pitch winding. As can be seen that the auxiliary slots have less influence on the torque in the machine with tooth-coil winding. This is due to the spatial harmonics in this machine is relatively low which means the smaller size auxiliary slots are required to compensate the spatial harmonics. As a result, the increased equivalent airgap length due to auxiliary slots is smaller in machine with tooth-coil winding.

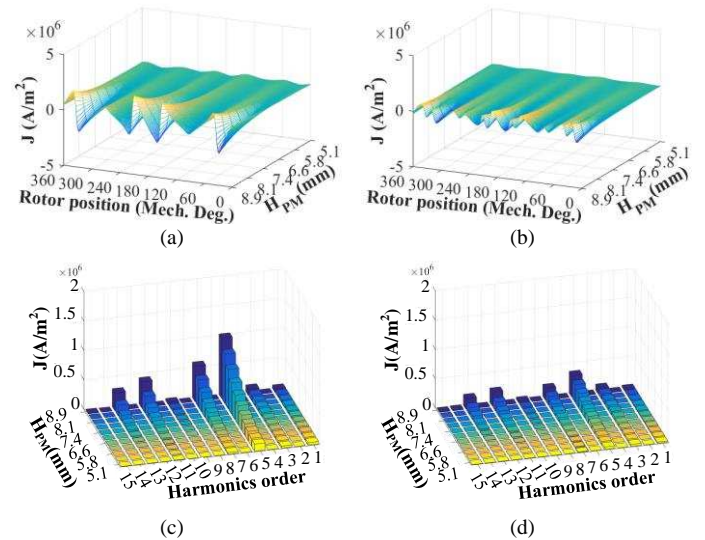


Fig. 22. Comparison of current density distributions of 6-slot/2-pole machine with full pitch winding. (a) and (b) Waveform of machine without and with auxiliary slots. (c) and (d) Spectra of machine without and with auxiliary slots.

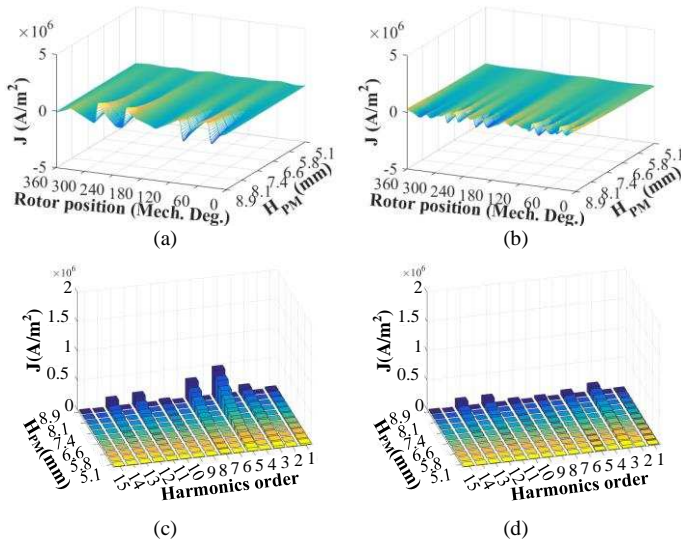


Fig. 23. Comparison of current density distributions of 6-slot/2-pole machine with tooth-coil winding. (a) and (b) Waveforms of machine without and with auxiliary slots. (c) and (d) Spectra of machine without and with auxiliary slots.

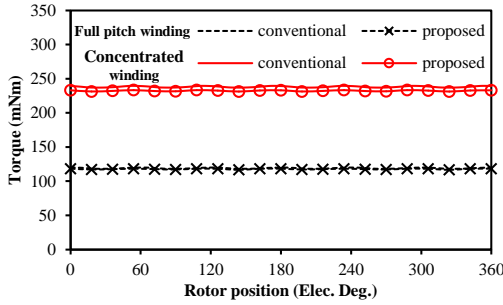


Fig. 24. Rated on-load torque of 6-slot/2-pole machines with different currents.

In contrast, the torque reduction in the 3-slot machines is 4.8% as shown in Fig. 12, which is much higher than that in 6-slot machines, since the spatial harmonics content in 3-slot machines are much higher due to asymmetric windings. The rated on-load airgap flux densities are shown in Fig. 25, and the comparison of total harmonic distortion (THD) is listed in Table V. As a result, it can be seen that the abundant even low order spatial harmonics due to asymmetric windings result in higher spatial harmonics, and hence, higher THD, which means larger auxiliary slots are required in 3-slot machines. Consequently, the torque reduction is higher in 3-slot machines.

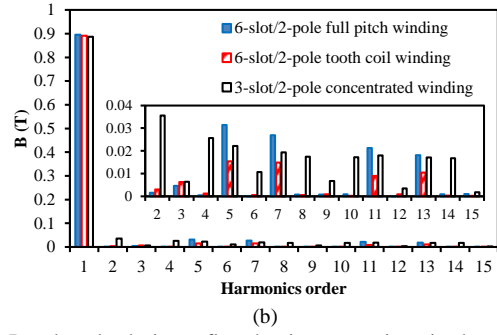
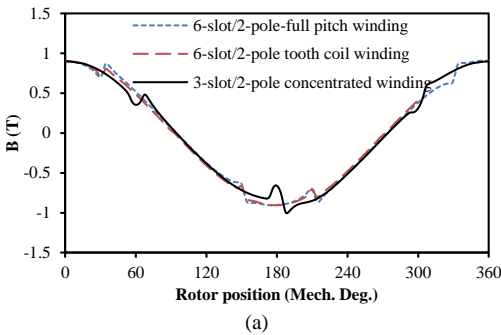


Fig. 25. Rated on-load airgap flux density comparison in the conventional machine. (a) Waveforms (b) Spectra.

TABLE VI
TOTAL HARMONIC DISTORTION IN CONVENTIONAL MACHINES WITH DIFFERENT SLOT/POLE COMBINATIONS AND WINDING CONFIGURATIONS

| Configuration | THD (%) |
|----------------------------------|---------|
| 3-slot/2-pole tooth-coil winding | 7.56% |
| 6-slot/2-pole full pitch winding | 5.61% |
| 6-slot/2-pole tooth-coil winding | 2.98% |

VIII. EXPERIMENTAL VALIDATION

In order to validate the numerically predicted results, the experiments for back EMF and static torque are carried out. The pictures of conventional and proposed machines are shown in Fig. 26. Both conventional and proposed 3-slot/2-pole machines have been built with the airgap length of 0.6mm.

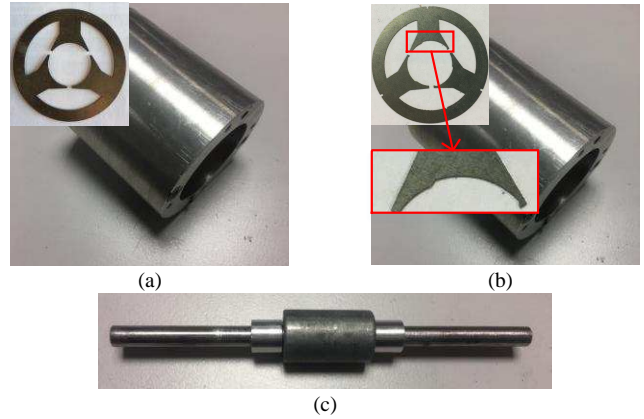


Fig. 26. Photos of 3-slot/2-pole prototype machines. (a) Stator of conventional machine. (b) Stator of proposed machine. (c) Rotor.

It should be noticed that due to the small size, low output torque and high rotating speed, the total loss and each loss component are very hard to be measured accurately. Nevertheless, several main electromagnetic performances, i.e. the open-circuit back EMF and static torque, are tested to verify the correctness of the FE results.

The open-circuit back-EMFs at 1000r/min are measured and compared with 2D and 3D FE predicted results in Fig. 27. It can be seen that the great agreement is observed. In addition, the 3D simulation results are closer to the test results, since it has taken the end effect into consideration. The slight difference is mainly due the manufacturing error, etc. Moreover, the difference between the conventional and proposed machines is small which means the auxiliary slots have slight influence on the back EMF.

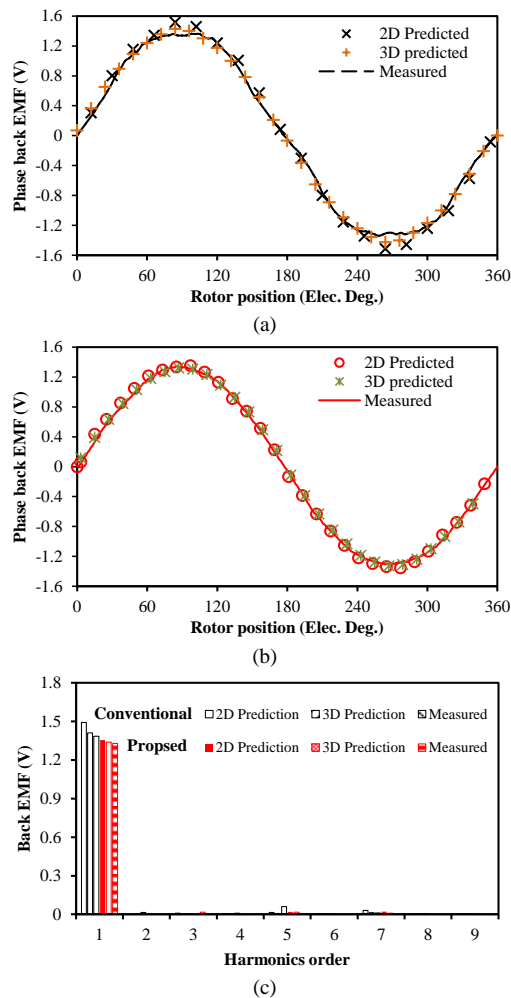


Fig. 27. Comparison of FE-predicted and measured back EMFs at 1000r/min. (a) Waveforms of conventional machine. (b) Waveforms of proposed machine. (c) Spectra.

In addition, the static torque of both machines are measured, which is defined as the torque with fixed input current as $I_B = I_c = -\frac{1}{2}I_a$. The variation of rated static torque with different rotor position is shown in Fig. 28 (a) and the maximum torque with different input current is shown in Fig. 28 (b). It can be seen that the difference between the predicted and measured values is very small, and it shows the conventional machine has slightly higher output torque comparing with the proposed one.

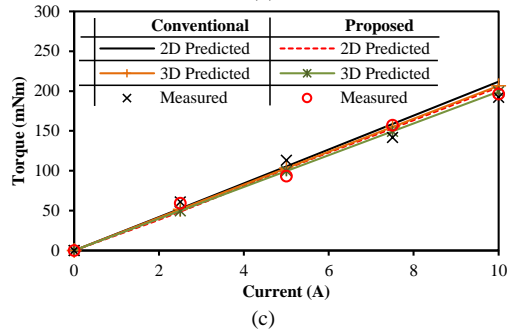
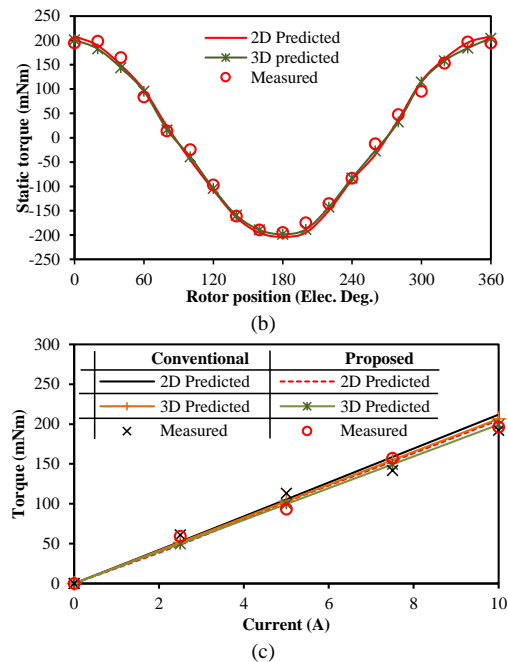
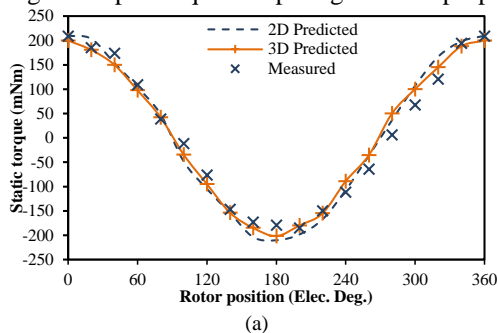


Fig. 28. Comparison of FE-predicted and measured static torques with different rotor positions and q-axis currents. (a) Torque in the conventional machine with different rotor positions and $I_q = 10$ A. (b) Torque in the proposed machine with different rotor positions and $I_q = 10$ A. (c) Maximum on-load torque with different I_q .

IX. CONCLUSION

In this paper, a new method has been proposed to reduce the magnet eddy current loss in a high speed machine. The 3-slot/2-pole machine with concentrated winding has been investigated at first. The air-gap flux density has been analyzed by a MMF-permeance model accounting for the slotted effect, it shows that the asynchronous harmonics produced by the armature field as well as by the conventional slots can be partially reduced with the harmonics caused by the optimized auxiliary slots, so that the magnet eddy current loss can be reduced significantly. Another point is that the auxiliary slots just increase the air-gap length slightly, and hence the reduction of output torque is also very small. However, this method also has limitations, the most important one is the working condition of the machine has great effect. In addition, the influence of airgap length and slot/pole combinations have been investigated as well, it shows that the machine with larger airgap could benefit more from the proposed method and this method is effective in all 3-slot and 6-slot machines.

REFERENCES

- [1] A. M. El-Refai, "Fractional-slot concentrated-windings synchronous permanent magnet machines: Opportunities and challenges," *IEEE Trans. Ind. Electron.*, vol. 57, no. 1, pp. 107–121, Jan. 2010.
- [2] D. Gerada, A. Mebarki, N. L. Brown, C. Gerada, A. Cavagnino, and A. Boglietti, "High-speed electrical machines: technologies, trends, and developments," *IEEE Trans. Ind. Electron.*, vol. 61, no. 6, pp. 2041–2059, 2014.
- [3] A. Borisavljevic, H. Polinder, and B. Ferreira, "Overcoming limits of high-speed PM machines," 18th Int. Conf. Electrical Machines (ICEM), 2008, pp. 1–6.
- [4] F. G. Zhang, G. H. Du, T. Y. Wang, G. W. Liu, and W. P. Cao, "Rotor retaining sleeve design for a 1.12-MW high-speed PM machine," *IEEE Trans. Ind. Appl.*, vol. 51, no. 5, pp. 3675–3685, Sep./Oct. 2015.

- [5] J. Ewanchuk, J. Salmon, and A. Knight, "Performance of a high-speed motor drive system using a novel multilevel inverter topology," *IEEE Trans. Ind. Appl.*, vol. 45, no. 5, pp. 1706–1714, Sep./Oct. 2009.
- [6] N. Bianchi, S. Bolognani, F. Luise, "Potentials and limits of high-speed PM motors," *IEEE Trans. Ind. Appl.*, vol. 40, No. 6, pp. 1570-1578, November/December 2004.
- [7] C. Bailey, D. M. Saban and P. Guedes-Pinto, "Design of High-Speed Direct-Connected Permanent-Magnet Motors and Generators for the Petrochemical Industry," *IEEE Trans. Ind. Appl.*, vol. 45, no. 3, pp. 1159-1165, May-June 2009.
- [8] E. Lovelace, et al., "Mechanical Design Considerations for Conventionally Laminated, High-Speed, Interior PM Synchronous Machine Rotors", *IEEE Trans. Ind. Appl.*, vol. 40, no. 3, pp. 806-812, May/June 2004.
- [9] Z. Q. Zhu, S. Ruangsinchaiwanich, and D. Howe, "Synthesis of cogging torque from a single stator slot in permanent magnet machines," *IEEE Trans. Ind. Appl.*, vol. 42, no. 3, pp. 650–657, May/June 2006.
- [10] M. Merdzan, J. J. H. Paulides, and E. A. Lomonova, "Comparative analysis of rotor losses in high-speed permanent magnet machines with different winding configurations considering the influence of the inverter PWM," in *Proc. 10th IEEE Int. Conf. Ecol. Vehicles Renew. Energies (EVER)*, Monte Carlo, Monaco, Mar./Apr. 2015, pp. 1–8.
- [11] S. Spas, G. Dajaku, and D. Gerling, "Eddy Current Loss Reduction in PM Traction Machines Using Two-Tooth Winding," *Vehicle Power and Propulsion Conference (VPPC)*, Oct. 2015, pp. 1-6.
- [12] H. Toda, Z. Xia, J. Wang, K. Atallah, and D. Howe, "Rotor Eddy Current Loss in Permanent Magnet Brushless Machines," *IEEE Trans. on Magn.*, vol. 40, no. 4, pp. 2104–2106, 2004.
- [13] S. S. Xue, H. P. Xu, and C. Fang, "The Effect of Stator Slot and Air Gap Length on High Speed Brushless PM Motor," *2012 7th int. conf. Power Electronics and Motion Control Conference (IPEMC)*, 2012, pp. 281-285.
- [14] J. Ede, Z. Zhu, and D. Howe, "Rotor resonances of high-speed permanent-magnet brushless machines," *IEEE Trans. Ind. Appl.*, vol. 38, no. 6, pp. 1542–1548, Nov. 2002.
- [15] I. Takahashi, T. Koganezawa, G. Su, and K. Ohya, "A super high speed PM motor drive system by a quasi-current source inverter," *IEEE Trans. Ind. Appl.*, vol. 30, no. 3, pp. 683–690, 1994.
- [16] Z. Belli and M. R. Mekideche, "Optimization of magnets segmentation for eddy current losses reduction in permanent magnets electrical machines," in *8th International Conference and Exhibition on Ecological Vehicles and Renewable Energies 2013 (EVER)*, 2013, pp. 1-7.
- [17] M. Mirzaei, A. Binder, and C. Deak, "3D analysis of circumferential and axial segmentation effect on magnet eddy current losses in permanent magnet synchronous machines with concentrated windings," *19th Int. Conf. on Electrical Machines (ICEM)*, Rome, Italy, Sep. 6–8, 2010.
- [18] K. Yamazaki, M. Shina, Y. Kanou, M. Miwa, and J. Hagiwara, "Effect of eddy current loss reduction by segmentation of magnets in synchronous motors: Difference between interior and surface types," *IEEE Trans. on Magn.*, Vol. 45, No. 10, pp.4756- 4959, 2009.
- [19] J. L. F. van der Veen, L. J. J. Offringa, and A. J. A. Vandenput, "Minimizing rotor losses in high-speed high-power permanent magnet synchronous generators with rectifier load," *IEEE Proc. Elect. Power Appl.*, vol. 144, no. 5, pp. 331–337, Sep. 1997.
- [20] W. Y. Huang, A. Bettayeb, R. Kaczmarek, and J. C. Vannier, "Optimization of magnet segmentation for reduction of eddy current losses in permanent synchronous machine," *IEEE Trans. Energy Convers.*, vol. 25, no. 2, pp. 381-387, 2010.
- [21] A. N. Marashi, K. Abbaszadeh, and F. R. Alam, "Analysis and reduction of magnet eddy current losses in surface mounted permanent magnet machines", *IEEE 22nd Iranian Conference on Electrical Engineering (ICEE 2014)*, pp. 782-786, 20-22 May 2014.
- [22] Z. Belli, "Optimization of stator slots shape for eddy current losses reduction in permanent magnets synchronous machine," *2014 9th Int. Conf. on Ecological Vehicles and Renewable Energies (EVER)*, 2014, pp. 1-7.
- [23] S. H. Chai, B. Y. Lee, J. J. Lee, and J. P. Hong, "Reduction eddy current loss design and analysis of in-wheel type vehicle traction motor," *2010 Int. Conf. on Electrical Machines and Systems (ICEMS)*, 2010, pp. 1264-1267.
- [24] S. Chaithongsuk, N. Takorabet, and S. Kreuawan, "Reduction of eddy-current losses in fractional-slot concentrated-winding synchronous PM motors," *IEEE Trans. on Magn.*, vol. 51, no. 3, 2015.
- [25] A. Binder, T. Schneider, and M. Klohr, "Fixation of buried and surface-mounted magnets in high-speed permanent-magnet synchronous machines," *IEEE Trans. Ind. Appl.*, vol. 42, no. 4, pp. 1031-1037, 2006.
- [26] G. Zhang, F. Wang, and Y. Shen, "Reduction of rotor loss and cogging torque of high speed PM machine by stator teeth notching," in *Proc. Int. Conf. Elect. Mach. Syst. (ICEMS)*, Seoul, Korea, Oct. 2007, pp. 856–859.
- [27] J. Ma, and Z. Q. Zhu, "Magnet eddy current loss reduction in a 3-slot/2-pole permanent magnet machine," *Int. Conf. on Electric Machines and Drives (IEMDC)*, 2017.
- [28] K. Wang, Z. Q. Zhu, and G. Ombach, "Synthesis of high performance fractional-slot permanent-magnet machines with coil-pitch of two slot-pitches," *IEEE Trans. Energy Convers.*, vol. 29, no. 3, pp. 758–770, May 2014...
- [29] W. Q. Chu and Z. Q. Zhu, "Average torque separation in permanent magnet synchronous machines using frozen permeability," *IEEE Trans. Magn.*, vol. 49, no. 3, pp. 1202–1210, Mar. 2013.